International Journal of Solids and Structures 49 (2012) 2195–2201

Contents lists available at SciVerse ScienceDirect

International Journal of Solids and Structures

journal homepage: www.elsevier.com/locate/ijsolstr

How to compute plastic zones of heterogeneous materials: A simple approach using classical continuum and fracture mechanics

Yunan Prawoto *

Faculty of Mechanical Engineering, Universiti Teknologi Malaysia, 81310 UTM, Skudai, Johor, Malaysia

ARTICLE INFO

Article history:
Received 9 March 2012
Received in revised form 25 April 2012
Available online 7 May 2012

Keywords:
Finite element
Homogenization
Fracture
Plastic zone

ABSTRACT

This is a short technical paper on how to use classical continuum and fracture mechanics to calculate the plastic zones caused by cracks on heterogeneous or composite materials. As an example, a sample consisting of an α-phase and β-phase is used. A crack is introduced to the sample, and stress is then applied. The plastic zone in front of the crack resulting from the applied stress is then calculated using commercial software. The concept uses two-level modeling: a global model using homogenized stiffness from a unit cell of heterogeneous material and a local model for the α-phase and β-phase. While this paper is written for general purposes, a concrete example using ferrite and martensite is also presented along with the experimental data. General agreement between the model and the experiment is observed. This method eliminates the need for a cumbersome analytical approach.

1. Introduction

Information about the plastic zones (PZ) in front of cracks can be very useful for evaluating the components used in oil refineries, automobiles and aircrafts (Oudad et al., 2009; Ramachandran, 2005), in terms of both ferrous and non-ferrous materials (Atas and Sayman, 2000; Bouiadjra et al., 2009; Xin et al., 2010; Yi et al., 2010). Understanding the plastic zone in front of a crack caused either by residual stress, applied loading or any other stresses can be very beneficial.

For decades, classical continuum mechanics have proven to be successful in predicting the shape and the size of the plastic zone in homogeneous materials. However, their application to heterogeneous materials has been cumbersome due to their analytical approach. When the shape of a material's multiphase constituents is simple, such as in the case of spheres, squares or ovals, an analytical solution can still be formulated. Unfortunately, it is rare that the shapes of the constituents are so simple. The majority of constituents have random shapes, especially those which occur naturally. Though several attempts to use other methods, including fractal theory, have been attempted (Carpinteri et al., 2004; Cherepanov et al., 1995; Epstein and Asniatycki, 2006; Kassner et al., 2005; Oden et al., 2003; Reddy and Rao, 2008; Wnuk and Yavari, 2008), these analytical approaches have often been very difficult and impractical to pursue.

With the advancing popularity of commercial finite element analysis programs, computer technology can obviate the need for difficult analytical approaches. Currently, researchers are able to simplify and manipulate the model. This short technical paper gives an example of how to manipulate the data so that a classical continuum mechanics approach can be used to study heterogeneous materials, even though it was originally developed for homogeneous materials.

2. Theory

Due to the technical nature of this paper, which relies on several different fields of knowledge, the theories related to this subject are briefly presented. Readers who are not familiar with these concepts are encouraged to consult elementary textbooks on mechanics, fracture mechanics, and mathematics.

2.1. Homogenization

The concept of homogenization has become accepted as a computational approach to heterogeneous materials (Aizawa et al., 2002; Lee et al., 1996; Prawoto, 2012). While the detailed theory is beyond the scope of this technical paper, a short introduction is presented here for the reader's convenience. In this theory, the local constitutive structure is taken to have a locally specified periodic unit cell, as shown in Fig. 1. Hence, every physical variable field on this material support can be expressed by a combination of its averaged part with a local disturbance, as depicted in part (b) of the figure. Assuming that the periodicity, ε, is sufficiently small, every physical field $u(x,y)$ can be represented by an asymptotic expansion in ε,

* Tel.: +60 167 279048; fax: +60 755 66159.
E-mail address: yunan.prawoto@gmail.com

0020-7683/$ - see front matter © 2012 Elsevier Ltd. All rights reserved.
http://dx.doi.org/10.1016/j.ijsolstr.2012.04.037

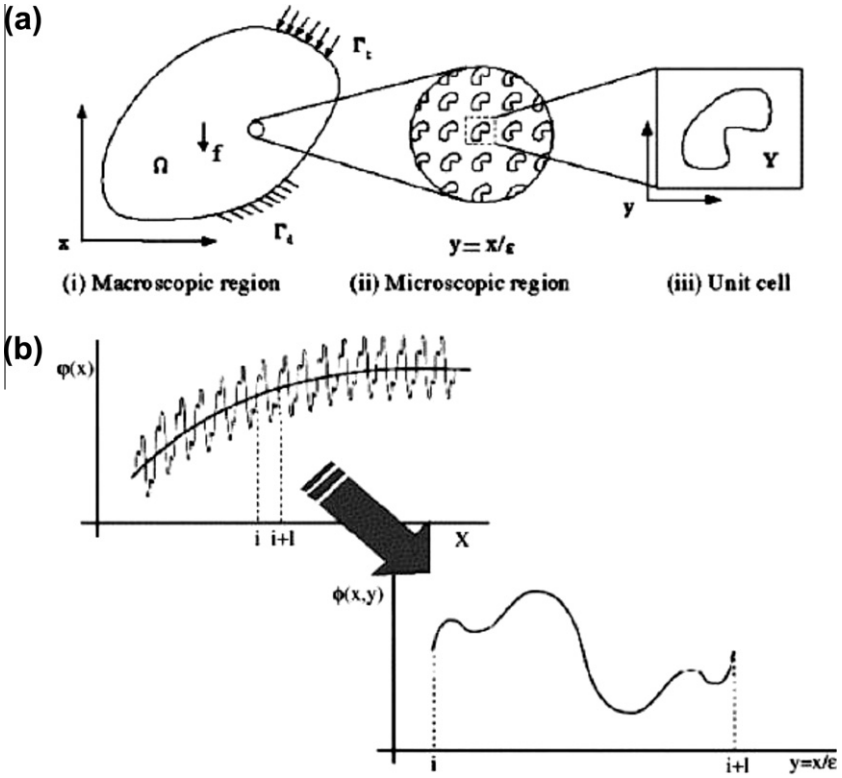

Fig. 1. (a) A frame of multi-scaling in materials using the homogenization theory. (b) Local deviation in the field variable to be embedded into the rationally smoothed distribution (Aizawa et al., 2002; Prawoto, 2012).

$$u(x,y) = u^0(x,y) + \varepsilon u^1(x,y) + \frac{1}{2}\varepsilon^2 u^2(x,y) + \cdots \text{ for } y \equiv x/\varepsilon \tag{1}$$

or

$$u(x,y) \cong u^0(x,y) + \varepsilon u^1(x,y) \tag{2}$$

where $\{u^0, u^1\}$ are, respectively, the functions for the averaged part and for the disturbance. Owing to the periodicity of function u in y, the following two equations are powerful tools:

$$\frac{\partial}{\partial x_i}u(x,y) = \frac{\partial u}{\partial x_i} + \frac{1}{\varepsilon}\frac{\partial u}{\partial y_i} \tag{3}$$

and

$$\lim_{x\to 0}\int_V u(x,y)dV = \int_V \frac{1}{|Y|}\left[\int_y u(x,y)dY\right]dV \tag{4}$$

where Y denotes the volume of the unit cell. These two equations (or forms similar to them) have also been frequently used in the computational approach to auxetic materials. To use this principle in FEA to compute the elastic modulus, recall the weak form of the linear elasticity finite element problem:

$$\int_\Omega E_{ijkl}\frac{\partial u_k}{\partial x_i}\frac{\partial v_i}{\partial x_j}d\Omega = \int_\Omega b_i v_i d\Omega + \int_\Gamma t_i v_i d\Gamma \tag{5}$$

Using the homogenization principle, we use x and y as microscale coordinates (see Fig. 1),

$$u(x,y) = u^0(x,y) + \varepsilon u^1(x,y) + \frac{1}{2}\varepsilon^2 u^2(x,y) + \cdots \text{ for } y \equiv x/\varepsilon \tag{6}$$

and

$$v(x,y) = v^0(x,y) + \varepsilon v^1(x,y) + \frac{1}{2}\varepsilon^2 v^2(x,y) + \cdots \text{ for } y \equiv x/\varepsilon \tag{7}$$

or

$$u(x,y) \cong u^0(x,y) + \varepsilon u^1(x,y) \tag{8}$$

and

$$v(x,y) \cong v^0(x,y) + \varepsilon v^1(x,y) \tag{9}$$

Meanwhile, the gradients of u and v are:

$$\begin{aligned}\nabla u(x,y) &= \nabla_x u^0(x,y) + \varepsilon\nabla_x u^1(x,y) + \varepsilon\nabla_y u^1(x,y)\\ \nabla v(x,y) &= \nabla_x v^0(x,y) + \varepsilon\nabla_x v^1(x,y) + \varepsilon\nabla_y v^1(x,y)\end{aligned} \tag{10}$$

Combining Eq. (5) with the above equations gives:

$$\begin{aligned}&\int_\Omega E_{ijkl}\left(\frac{\partial u_k^0}{\partial x_l} + \frac{\partial u_k^1}{\partial x_l}\right)\left(\frac{\partial v_i^0}{\partial x_j} + \frac{\partial v_i^1}{\partial x_j}\right)d\Omega + \varepsilon\int_\Omega E_{ijkl}\left[\frac{\partial u_k^1}{\partial x_i}\left(\frac{\partial u_k^0}{\partial x_l} + \frac{\partial u_k^1}{\partial x_l}\right)\right.\\ &\left.+\left(\frac{\partial v_i^0}{\partial x_j} + \frac{\partial v_i^1}{\partial x_j}\right)\frac{\partial v_i^1}{\partial x_j}\right]d\Omega + \varepsilon^2\int_\Omega E_{ijkl}\frac{\partial u_k^1}{\partial x_i}\frac{\partial v_i^1}{\partial x_j}d\Omega\\ &= \int_\Omega b_i(v_i^0 + \varepsilon v_i^1)d\Omega + \int_\Gamma t_i(v_i^0 + \varepsilon v_i^1)d\Gamma\end{aligned} \tag{11}$$

When $\varepsilon \to 0$, this becomes

$$\int_\Omega E_{ijkl}\left(\frac{\partial u_k^0}{\partial x_l} + \frac{\partial u_k^1}{\partial x_l}\right)\left(\frac{\partial v_i^0}{\partial x_j} + \frac{\partial v_i^1}{\partial x_j}\right)d\Omega = \int_\Omega b_i v_i^0 d\Omega + \int_\Gamma t_i v_i^0 d\Gamma \tag{12}$$

and can be separated to:

$$\begin{aligned}&\lim_{x\to 0}\int_\Omega E_{ijkl}\left(\frac{\partial u_k^0}{\partial x_l} + \frac{\partial u_k^1}{\partial x_l}\right)\left(\frac{\partial v_i^0}{\partial x_j}\right)d\Omega\\ &= \lim_{x\to 0}\int_\Omega b_i v_i^0 d\Omega + \int_\Gamma t_i v_i^0 d\Gamma\end{aligned} \tag{13}$$

and

$$\lim_{x\to 0}\int_\Omega E_{ijkl}\left(\frac{\partial u_k^0}{\partial x_l} + \frac{\partial u_k^1}{\partial x_l}\right)\left(\frac{\partial v_i^1}{\partial x_j}\right)d\Omega = 0 \tag{14}$$

Using Eq. (11), we can rewrite this as

$$\lim_{x\to 0}\int_\Omega \Phi(x,y)d\Omega = \int_\Omega \frac{1}{|Y|}\left[\int_y \Phi(x,y)dY\right]dV \tag{15}$$

Eqs. (13) and (14) eventually become:

$$\int_\Omega \frac{1}{|Y|}\int_Y E_{ijkl}\left(\frac{\partial u_k^0}{\partial x_l}+\frac{\partial u_k^1}{\partial x_l}\right)\left(\frac{\partial v_i^0}{\partial x_j}\right)dYd\Omega = \int_\Omega b_i v_i^0 d\Omega + \int_\Gamma t_i v_i^0 d\Gamma \tag{16}$$

and

$$\int_\Omega \frac{1}{|Y|}E_{ijkl}\left(\frac{\partial u_k^0}{\partial x_l}+\frac{\partial u_k^1}{\partial x_l}\right)\left(\frac{\partial v_i^1}{\partial x_j}\right)dYd\Omega = 0 \tag{17}$$

Introducing a separation of variables to satisfy this based on linear elasticity,

$$u_i^1(x,y) = -\chi_i^{pq}(\underline{y})\frac{\partial u_p^0}{\partial x_q}(\underline{x}) \tag{18}$$

where χ_p^{kl} is the microscale parameter. This can be obtained by combining Eqs. (18) and (17):

$$\int_\Omega \frac{1}{|Y|}\int_Y \left(E_{ijkl}-E_{ijkl}\frac{\partial \chi_i^{pq}}{\partial y_j}\right)\left(\frac{\partial v_i^1}{\partial y_j}\right)dY\frac{\partial u_k^0}{\partial x_l} = 0 \tag{19}$$

Therefore, our weak form becomes

$$\int_\Omega E_{ijkl}\left(\frac{\partial u_k^0}{\partial x_l}\right)\left(\frac{\partial v_i^0}{\partial x_j}\right)d\Omega = \int_\Omega b_i v_i^0 d\Omega + \int_\Gamma t_i v_i^0 d\Gamma \tag{20}$$

where the homogenized tensor of elasticity is

$$E_{ijkl}^H = \frac{1}{|Y|}\int_Y \left(E_{ijkl}-E_{ijpq}\frac{\partial \chi_p^{kl}}{\partial y_q}\right)dY \tag{21}$$

Therefore, the homogenization concept is highly applicable to heterogeneous materials. A unit cell can be chosen to represent the structure. Skeptics may say that this approach still does not work for natural structures, but in reality, it demonstrates a compromise approach that has been proven to be better than a simple rule of mixture, which does not accommodate the shapes of the constituents (Prawoto, 2012).

2.2. Stress intensity factor

The concepts of fracture mechanics are concerned with developing methods to predict the load-carrying capabilities of structures containing cracks. This fracture mechanics approach is based on a mathematical description of the characteristic stress field surrounding a crack in a loaded body.

To explore the characteristics of the stress field surrounding a crack in a loaded body, one can start with the Westergaard function. The Westergaard function is a complex solution to the Airy stress function. To do this, consider a coordinate system x, y, z in a stressed solid. At each point (x,y,z), one can define the stresses σ_x, σ_y, σ_z, τ_{xy}, τ_{xz}, and τ_{yz}. Neglecting the body forces, for two-dimensional problems, the equilibrium equations are

$$\frac{\partial \sigma_x}{\partial x}+\frac{\partial \tau_{xy}}{\partial y} \text{ and } \frac{\partial \sigma_y}{\partial y}+\frac{\partial \tau_{xy}}{\partial x} \tag{22}$$

Also recall their relations with the elastic strain:

$$\varepsilon_x = \frac{\partial u}{\partial x}, \quad \varepsilon_y = \frac{\partial v}{\partial y}, \quad \gamma_{xy} = \frac{\partial u}{\partial y}+\frac{\partial v}{\partial x} \tag{23}$$

The equilibrium equation in (22) is automatically satisfied if

$$\sigma_x = \frac{\partial^2 \psi}{\partial y^2}, \quad \sigma_y = \frac{\partial^2 \psi}{\partial x^2}, \quad \tau_{xy} = \frac{\partial^2 \psi}{\partial x \partial y} \tag{24}$$

with the stress–strain relation

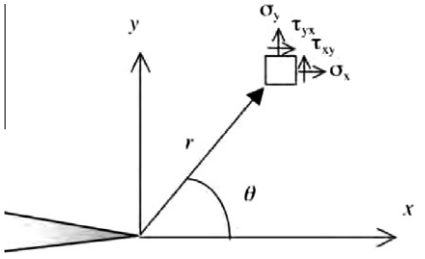

Fig. 2. Basic usage of linear elastic fracture mechanics method (Prawoto, 2009).

$$E\varepsilon_x = \sigma_x - \nu\sigma_y, \quad E\varepsilon_y = \sigma_y - \nu\sigma_x, \quad \tau_{xy} = \frac{E\gamma_{xy}}{2(1+\nu)} \tag{25}$$

The function ψ is called the Airy stress function. With extensive mathematical manipulation (Prawoto, 2009, 2011), the stress singularity in front of a crack can then be expressed by

$$\sigma_{ij} = \frac{K_I}{\sqrt{2\pi r}}f_{ij}(\theta) \tag{26}$$

where r and θ are the polar coordinates of a point with respect to the crack tip, and K_I is the stress intensity factor (see Fig. 2).

2.3. J-integral

While the discussion in the former section is limited to linear elastic mechanics, this section covers non-linear elastics. The J-integral is one way to calculate the strain energy release rate, or work (energy) per unit fracture surface area (Anderson, 1995). The J-integral is equal to the strain energy release rate for a crack in a body subjected to loading under quasi-static conditions (see Fig. 3). Its simplified two-dimensional form is

$$J \cong \int_\Gamma \left[Wdx_2 - t\cdot\frac{\partial u}{\partial x_1}ds\right] \tag{27}$$

where x_1 is the crack direction, x_2 is perpendicular to the crack direction, W is the strain energy density, and n is the surface traction vector. Its general expression is known by:

$$J \cong \int_\Gamma \left[Wn_i - n_j\sigma_{jk}\cdot\frac{\partial u_k}{\partial x_1}\right]d\Gamma \tag{28}$$

where

$$T = n_j\sigma_{jk} \tag{29}$$

and

$$W = \int_0^{\varepsilon_{ij}} \sigma_{ij}d\varepsilon_{ij} \tag{30}$$

This represents the strain energy release rate of non-linear elastic materials, as shown in the following,

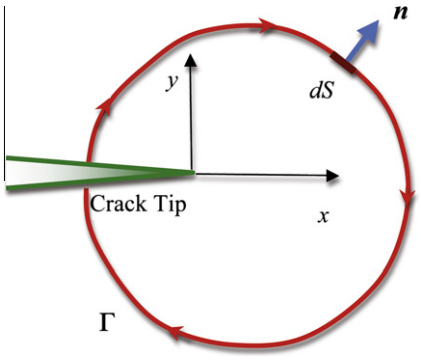

Fig. 3. Basic usage of non-linear fracture mechanics concept of the J-integral.

$$J \equiv -\frac{d\Pi}{dA} \tag{31}$$

where Π is the potential energy of the cracked body.

For the sake of simplicity, the scope of this technical paper is limited to linear elastic and elastic–plastic cases. Due to the unidirectional nature of this topic, the term elastic–plastic is treated as non-linear elastic. For these purposes, the term elastic–plastic becomes indistinguishable from non-linear elastic.

Let the curvature of the non-linear elastic take the following form.

$$\sigma = \sigma_0 \left(\frac{\varepsilon}{\varepsilon_0}\right)^{\frac{1}{n}} \tag{32}$$

Here, n is the hardening index. In this case, mimicking the Rice–Rosengren formulation, referred to from now on as the HRR (Hutchinson–Rice–Rosengren (He and Hutchinson, 1981; Rice and Rosengren, 1968)) formulation, the following stress, strain, and displacement fields at a point near the crack tip (θ, r) must be true:

$$\sigma_{ij} = \sigma_0 \left(\frac{J}{\sigma_0 \varepsilon_0 r}\right)^{\frac{1}{n}} \Sigma_{ij}(\theta, n) \tag{33}$$

$$\varepsilon_{ij} = \varepsilon_0 \left(\frac{J}{\sigma_0 \varepsilon_0 r}\right)^{\frac{n}{n+1}} E_{ij}(\theta, n) \tag{34}$$

$$u_i = J \left(\frac{\sigma_0 \varepsilon_0 r}{J}\right)^{\frac{1}{n+1}} U_{ij}(\theta, n) \tag{35}$$

where Σ_{ij}, E_{ij}, and U_{ij} are dimensionless functions.

Rewriting our definition of the J-integral, Eq. (28),

$$J = \int_{\Gamma} \left[\frac{n}{n+1} \sigma_0 \varepsilon_0 \left(\frac{3 S_{ij} S_{ij}}{2 \sigma_0}\right)^{n+1} \delta_{j1} - \sigma_{ij} \frac{\partial u_i}{\partial x_1}\right] m_j ds \tag{36}$$

where the deviatoric stress is

$$S_{ij} = \sigma_{ij} - \frac{\sigma_{kk} \delta_{ij}}{3} \tag{37}$$

Recall that this means for a linear elastic case, $n = 1$, and for a perfectly plastic case, $n = \infty$.

3. Computational approach

We have designated Eq. (21) for averaging the heterogeneous materials, Eq. (26) for stress description near the crack in linear elasticity, and its comparable governing rule of Eq. (33) for non-linear elasticity (sometimes referred to as elasto-plasticity, though strictly speaking they are different). The theoretical plastic zone shape varies depending on the distance along the crack front compared to a free surface. The two extreme cases appear on the surface and in the middle of a thick sample. On the surface, which is governed by plane stress, the plastic zone shape differs from inside the sample, where it is governed by plane strain. Here, using the same concept, both two-dimensional modeling and three-dimensional modeling were performed. The latter is only described briefly due to its similarity to the former. For this purpose, the computation for a material with two different phases, namely α and β phases, is highlighted. From time to time, this note refers to previously published papers (Prawoto, 2009; Prawoto et al., 2009, 2011).

3.1. Modeling procedure

The model here is a heterogeneous material, having a constituent of α-phase inside a β-phase matrix. As a test specimen, a CT (compact tension) specimen according to the ASTM E647 (ASTM, 2008a) standard was chosen. The following steps were taken:

- Application of homogenization theory to the heterogeneous material.
  ⇒ Eq. (21).
- Use the material characteristics to treat the global heterogeneous material as a homogenized object, followed by FEA model verification.
  ⇒ Eqs. (26) and (33).⇒ASTM (ASTM, 2008a,b).
- Use the material characteristics to treat the global heterogeneous material as a homogenized object.
  ⇒ Non-linear-elastic or elasto-plastic analysis. Eq. (32).
- Obtain the output of the global model and use it as a boundary condition to compute the local model with the heterogeneous material.
  ⇒ Use sub-modeling technique.

3.1.1. Application of homogenization theory to heterogeneous material

The first step of model creation is the application of the homogenization theory. This can be achieved by digitizing a microstructure obtained by an SEM or an optical microscope. For two-dimensional modeling, the model can be made either as a plane stress or a plane strain. For three-dimensional modeling, several commercial packages are available to construct it from multiple slices of picture files (e.g., Amira, which is popular among biomedical engineers/researchers). The unit cell can be created by placing two mirrors to guarantee the continuity of the boundary conditions (see Fig. 4). As an example, Young's modulus, E [GPa], was 180, and the Poissons ratio, ν, was 0.32. For the α-phase and the β-phase, E was 210 GPa and ν was 0.31. After applying the homogenization theory, the unit cell has a stiffness matrix of

$$\begin{bmatrix} E^H_{1111} & E^H_{1122} & 0 \\ E^H_{2211} & E^H_{2222} & 0 \\ 0 & 0 & E^H_{1212} \end{bmatrix} = \begin{bmatrix} 205.58 & 64.24 & 0 \\ 64.24 & 205.58 & 0 \\ 0 & 0 & 70.67 \end{bmatrix} \tag{38}$$

This stiffness matrix can then be used to construct the homogenized global model (next step). It is important to note that the application of the homogenization theory to obtain the stiffness is not mandatory. Depending on the accuracy one needs and depending on the extent to which one might want to consider the influence of the shape of each constituent, other methods can be used. The decision on whether to use the homogenization concept or other methods, such as the regular rule of mixture, is typically dependent upon the shape of the constituent because the rule of mixture does not take into account the stress amplification caused by constituent shapes; it is a simple volumetric averaging. The closer the constituent structure is to a circle or sphere, the more accurate the rule of mixture. The farther away the structure veers from a sphere, especially if the shape is sharp, the less accurate the rule of mixture. In such a case, the homogenization theory is advantageous.

3.1.2. The use of the material characteristics to treat global heterogeneous material as a homogenized object, followed by FEA model verification

In this step, the stiffness used was that of Eq. (38). The stress intensity factor, K, can be used for verification. For a compact tension specimen, the relation between the applied load, P, and K is as follows (ASTM, 2008a,b):

$$K = \frac{P}{B\sqrt{W}} \frac{2+\alpha}{(1-\alpha)^{3/2}} (0.886 + 4.64\alpha - 13.32\alpha^2 + 14.72\alpha^3 - 5.6\alpha^4) \tag{39}$$

where B and W represent specimen thickness and width, respectively, α is the relative crack length (a/W), and P is the applied load. For this analysis, an elastic material was used because the plastic zone is not studied at this step. The following values were used for both the analytical verification and the modeling: $\alpha = 0.45$, $W = 38.1$ [mm], and B = 10 [mm]. For this global model, the element

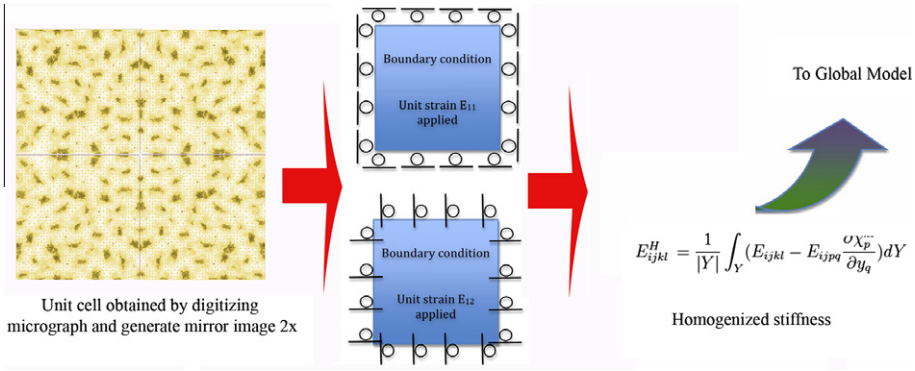

Fig. 4. Implementation of the homogenization theory on the unit cell created based on a real microstructure (10% of α-phase inside the β-phase matrix).

types used were CPE3 (3-node linear element) and CPE4R (4-node bilinear element, with reduced integration) with the applied load $P = 200$ [N]. For example, from this estimation result, it was found that the plastic zone was approximately 1.8 [mm] in height. At this point, one can choose to either lower the applied load until the desired size of the plastic zone is achieved or adjust the size of the local model to be slightly larger than the approximate plastic zone obtained at this step. For three-dimensional computations the basic principle is the same. Element types such as C3D8R (An 8-node linear brick with reduced integration) can be used.

3.1.3. The use of the material characteristics to treat global heterogeneous material as a homogenized object

The same model created in the previous step can be used here. The main point in this step is to adjust the applied loading. In this example, the area of interest is 1 $[mm]^2$ of area for the two-dimensional model and 1 $[mm]^3$ of volume is needed for the three-dimensional model. In such cases, the loading can then be lowered, e.g., to $P = 100$ [N]. Readers can either adjust the loading or the size of the local model according their needs.

3.1.4. Obtain the output of the global model, use it as a boundary condition to compute the local model with heterogeneous material

The sub-modeling technique is typically used to study a local part of a model with a refined mesh, based on the FEA result from a global model with a coarse mesh. There are two steps for sub-modeling: (1) Perform an analysis of a global (whole) model to find the boundary conditions for a local area (previous step). (2) Perform an analysis of a local model based on interpolation of the solution from the global model (this step). Displacement of the local model boundary is automatically interpolated from the result of the global model. The results of the von Mises stress and plastic zone are shown in Figs. 5 and 6.

4. Comparison of the modeling with the experimental data

Because the exact theoretical solution for heterogeneous material cannot be computed based on classical continuum mechanics,

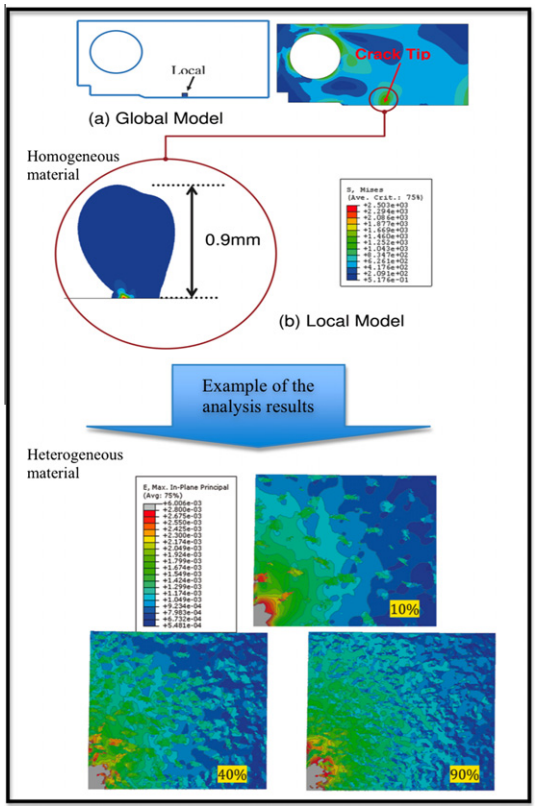

Fig. 5. Example of the plastic zone calculation with a two-dimensional method (Prawoto et al., 2009).

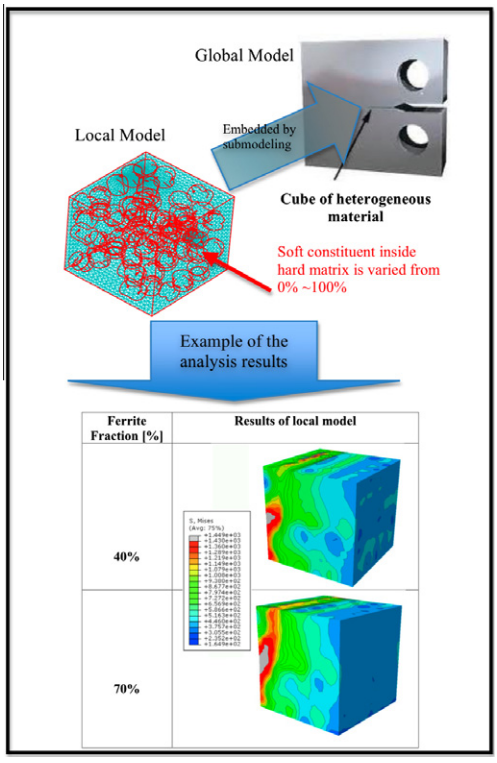

Fig. 6. Example of the plastic zone calculation with a three-dimensional method (Prawoto et al., 2011).

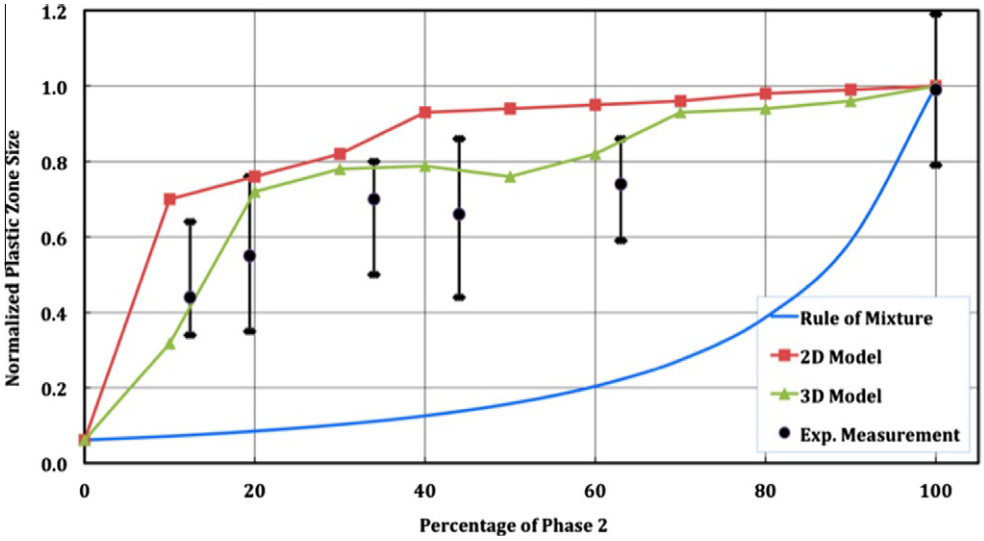

Fig. 7. Experimental verification with X-ray diffraction machine.

the theoretical solutions were based on two homogeneous materials. The harder constituent (β) gave a lower bound and the softer constituent produced an upper bound. Using the simple rule of mixture, the heterogeneous material yield strength was then calculated. Then, the plastic zone size can be calculated analytically. For simplicity, the plastic zone was computed only at the surface of the material. Therefore, the plain strain condition applies. Using Eqs. (26) and (33), the plastic zones in front of the crack and above the crack were calculated separately, and then the rule of mixture was applied. Fig. 7 shows the combined data. The result is normalized with respect to its maximum value, which is the upper bound of the plastic zone obtained analytically when 100% of the constituent is soft material (α-phase). It is worth noting that because the material here is AISI 10B21, which is a soft spring material, the percentage of the soft material could not be made to be exactly equal to the target. While these achievements and the metallurgical data remain confidential to the data supplier, the plastic zone size measurement method used can be briefly shared. Mimicking the peak-broadening concept previously used by the author (Prawoto and Winholtz, 2000), Rigaku X-ray diffraction was used. Due to the nature of the equipment, the error bar shown is somewhat large. The figures show that the computational results using both two-dimensional methods and three-dimensional methods end up with similar trends. This trend is also supported by the experimental results. Compared with the rule of mixture line, however, the trend is quite different. This is seemingly because in the rule of mixture, the second phase is always assumed to have no influence in raising the stress. However, in the actual microstructure, the shape is almost random; the shapes are nowhere near spherical, and therefore act to raise the stress, eventually leading to a larger plastic zone.

5. Conclusion

Manipulation methods that enable one to use classical continuum mechanics in heterogeneous materials were presented. As an example, the calculation of the plastic zone in front of a cracked member with an applied stress load was carried out. The results were found to be satisfactory. This concept can also be extended to other materials and other purposes. As these computational tools become easier to use, researchers outside this computational area, such as materials scientists, would be well advised to employ them. This approach enables researchers to avoid reliance on cumbersome analytical procedures that are sometimes impossible to execute.

References

Aizawa, T., Prawoto, Y., Tsumori, F., 2002. Coupled, macro-micro modeling for hot deformation and sintering. J. Comput. Appl. Math. 149, 307–324.
Anderson, T., 1995. Fracture Mechanics: Fundamentals and Applications, 2nd ed. CRC Press.
ASTM. 2008a. Standard test method for measurement of fatigue crack growth rates, in: ASTM:E647. ASTM International Publisher, West Conshohocken, PA.
ASTM. 2008b. Standard test methods for tension testing of metallic materials, in: ASTM:E8. ASTM International Publisher, West Conshohocken, PA.
Atas, C., Sayman, O., 2000. Elastic-plastic stress analysis and expansion of plastic zone in clamped and simply supported aluminum metal-matrix laminated plates. Comput. Struct. 49, 9–19.
Bouiadjra, B.B., Elmeguenni, M., Benguediab, M., Belhouari, M., Nait-Abdelaziz, M., 2009. Numerical estimation of the effects of microcavities on the plastic zone size ahead of the crack tip in aluminum alloy 2024 t3. Mat. Des. 30, 752–757.
Carpinteri, A., Chiaia, B., Cornetti, P., 2004. A fractal theory for the mechanics of elastic materials. Mat. Sci. Eng. A 365, 235–240.
Cherepanov, G.P., Balankin, A.S., Ivanova, V.S., 1995. Fractal fracture mechanics: A review. Eng. Frac. Mech. 51, 997–1033.
Epstein, M., Asniatycki, J., 2006. Fractal mechanics. Phys. D Nonlin. Phen. 220, 54–68.
He, M., Hutchinson, J., 1981. The penny-shaped crack and the plane strain crack in an infinite body of power-law material. J. Appl. Mech. 48, 830–840.
Kassner, M.E., Nemat-Nasser, S., Suo, Z., Bao, G., Barbour, J.C., Brinson, L.C., Espinosa, H., Gao, H., Granick, S., Gumbsch, P., Kim, K.S., Knauss, W., Kubin, L., Langer, J., Larson, B.C., Mahadevan, L., Majumdar, A., Torquato, S., van Swol, F., 2005. New directions in mechanics. Mech. Mater. 37, 231–259.
Lee, J., Choi, J.B., Choi, K., 1996. Application of homogenization fem analysis to regular and re-entrant honeycomb structures. J. Mater. Sci. 31, 4105–4110.
Oden, J., Belytschko, T., Babuska, I., Hughes, T., 2003. Research directions in computational mechanics. Comput. Meth. Appl. Mech. Eng. 192, 913–922.
Oudad, W., Bouiadjra, B.B., Belhouari, M., Touzain, S., Feaugas, X., 2009. Analysis of the plastic zone size ahead of repaired cracks with bonded composite patch of metallic aircraft structures. Comput. Mat. Sci. 46, 950–954.
Prawoto, Y., 2009. Designing steel microstructure based on fracture mechanics approach. Mat. Sci. Eng. A 507, 74–86.
Prawoto, Y., 2011. Application of Linear Elastic Fracture Mechanics in Materials Science and Engineering. Lulu Enterprise, Raleigh NC.
Prawoto, Y., 2012. Seeing auxetic materials from mechanics point of view: A structural review on the negative poisson's ratio. Comput. Mat. Sci. 58, 140–153.
Prawoto, Y., Idris, R., Kamsah, N., Tamin, N., 2009. Two-dimensional modeling to compute plastic zone in front of compact tension sample of a multiphase material. Comput. Mat. Sci. 47, 482–490.
Prawoto, Y., Idris, R., Kamsah, N., Tamin, N., 2011. Three-dimensional modeling to compute plastic zone in front of crack in compact tension sample of multiphase material. Comput. Mater. Sci. 50, 1499–1503.
Prawoto, Y., Winholtz, R., 2000. The growth rate and plastic zone size variations of a fatigue crack grown in a tensile residual stress field. In: Proceedings of the Eighth International Conference on Nuclear Engineering – American Society of Mechanical Engineers, paper# 8785.
Ramachandran, V., 2005. Failure analysis of engineering structures: methodology and case histories. ASM International.
Reddy, R., Rao, B., 2008. Stochastic fracture mechanics by fractal finite element method. Comput. Meth. Appl. Mech. Eng. 198, 459–474.
Rice, J., Rosengren, G., 1968. Plane strain deformation near a crack tip in a power-law hardening material. J. Mech. Phys. Sol. 16, 1–12.

Wnuk, M.P., Yavari, A., 2008. Discrete fractal fracture mechanics. Eng. Frac. Mech. 75, 1127–1142.
Xin, G., Hangong, W., Xingwu, K., Liangzhou, J., 2010. Analytic solutions to crack tip plastic zone under various loading conditions. Eur. J. Mech. A/Solids 29, 738–745.
Yi, H., Jingjie, C., Gang, L., 2010. A new method of plastic zone size determined based on maximum crack opening displacement. Eng. Frac. Mech. 77, 2912–2918.